Available online at www.sciencedirect.com
ScienceDirect
Physics Letters B 652 (2007) 169–173
PHYSICS LETTERS B
www.elsevier.com/locate/physletb

Quadrupole collectivity in silicon isotopes approaching neutron number $N = 28$

C.M. Campbell [a,b,*], N. Aoi [c], D. Bazin [a], M.D. Bowen [a,b], B.A. Brown [a,b], J.M. Cook [a,b], D.-C. Dinca [a,b], A. Gade [a,b], T. Glasmacher [a,b], M. Horoi [d], S. Kanno [e], T. Motobayashi [c], L.A. Riley [f], H. Sagawa [g], H. Sakurai [c], K. Starosta [a,b], H. Suzuki [h], S. Takeuchi [c], J.R. Terry [a,b], K. Yoneda [c], H. Zwahlen [a,b]

[a] *National Superconducting Cyclotron Laboratory, Michigan State University, East Lansing, MI 48824, USA*
[b] *Department of Physics and Astronomy, Michigan State University, East Lansing, MI 48824, USA*
[c] *RIKEN Nishina Center for Accelerator-Based Science, 2-1 Hirosawa, Wako, Saitama 351-0198, Japan*
[d] *Physics Department, Central Michigan University, Mount Pleasant, MI 48859, USA*
[e] *Department of Physics, Rikkyo University, 3-34-1 Nishi-Ikebukuro, Toshima, Tokyo 171-8501, Japan*
[f] *Department of Physics and Astronomy, Ursinus College, Collegeville, PA 19426, USA*
[g] *Center for Mathematical Sciences, University of Aizu, Aizu-Wakamatsu, Fukushima 965-8560, Japan*
[h] *Department of Physics, University of Tokyo, Tokyo 1130033, Japan*

Received 14 March 2007; received in revised form 11 June 2007; accepted 3 July 2007

Available online 6 July 2007

Editor: D.F. Geesaman

Abstract

Quadrupole deformation parameters, $|\beta_{2,(p,p')}|$, have been deduced for ^{36,38,40}Si from measured inelastic proton-scattering cross sections. Due to the strong $Z = 14$ subshell gap, low-lying quadrupole collectivity in these nuclei is attributed to the excitation of valence neutrons. Enhanced collectivity at $N = 26$ indicates a reduced $N = 28$ shell gap at large neutron excess in this chain of isotopes. Data are compared to large-scale shell-model calculations and prior Coulomb excitation measurements on ^{36,38}Si.

PACS: 25.40.Ep; 21.10.Re; 27.30.+z; 27.40.+z

Keywords: Inelastic proton scattering; Quadrupole collectivity; ^{36}Si; ^{38}Si; ^{40}Si

We report the study of quadrupole collectivity in the very neutron-rich nuclei ^{36,38,40}Si. Fast beams of these silicon isotopes were scattered off a liquid hydrogen target yielding inelastic excitation cross sections, $\sigma_{0_1^+ \to 2_1^+}$. These measurements reveal enhanced collectivity toward the end of the neutron $0f_{7/2}$ shell, bolstering the idea that the $N = 28$ shell gap narrows for silicon at this large neutron excess. Furthermore, differences in proton and neutron collectivity are studied for ^{36,38}Si. A comparison to large-scale shell-model calculations is provided.

The neutron-rich silicon isotopes ^{36,38,40}Si lie between neutron numbers 20 and 28. While $N = 20$ and $N = 28$ correspond to neutron shell closures near stability, intruder states from the next higher shell are found to cross the shell gap in the ground states of $N = 20$ isotones with $10 \leqslant Z \leqslant 12$ [1–3]. Also, the enhanced quadrupole collectivity observed in ^{44}S suggests a weakening of the $N = 28$ shell gap [4]. Ibbotson et al. measured 2_1^+ energies and corresponding $B(\mathrm{E2}\uparrow)$ values in ^{36,38}Si using intermediate-energy Coulomb excitation [5]. While both nuclei were found to be moderately collective, schematic shell-model calculations indicated that the observed collectivity could be explained without neutron excitations across the $N = 20$ shell gap. More recently, Liang et

* Corresponding author at: National Superconducting Cyclotron Laboratory, Michigan State University, East Lansing, MI 48824, USA.
E-mail address: campbell@nscl.msu.edu (C.M. Campbell).

0370-2693/$ – see front matter
doi:10.1016/j.physletb.2007.07.005

al. have used thin- and thick-target deep inelastic collisions to study the yrast level structure of ^{36}Si [6]. These levels are also consistent with shell-model calculations in which $N = 20$ is a closed shell. Thus, in the following we will consider $N = 20$ a closed shell in the silicon isotopes.

The size of the $N = 28$ shell gap at $Z < 18$, however, remains an open question. Since $N = 28$ is the first spin–orbit shell gap, it is important to understand its evolution far from stability. In the sulfur isotopic chain, enhanced quadrupole collectivity observed in ^{40,42,44}S could indicate a narrowing of the $N = 28$ shell gap [4]. However, using $(d, {}^3\mathrm{He})$ data taken on calcium isotopes [7], Cottle and Kemper found that as the neutron $0f_{7/2}$ orbital is filled the proton *sd*-shell orbitals shift relative to one another [8]. Specifically, the proton $1s_{1/2}$–$0d_{3/2}$ subshell gap narrows, but the proton $0d_{5/2}$–$1s_{1/2}$ subshell gap remains large. These findings are supported by a recent proton knockout study of neutron-rich $N = 28$ isotones [9]. In the neutron-rich sulfur isotopes, the reduced subshell gap frees protons to participate in collective motion and makes it difficult to tie an increased collectivity near $Z = 16$, $N = 28$ to a change in the neutron shell gap. To cleanly separate the contributions from valence protons and neutrons, we have measured quadrupole collectivity in the silicon isotopes, where the $Z = 14$ subshell gap remains large from $N = 20$ to $N = 28$. Here, we extend quadrupole collectivity measurements to ^{40}Si and observe greater collectivity at $N = 26$ than at $N = 22$, pointing to a possible narrowing of the $N = 28$ shell gap.

The experiment was performed at the National Superconducting Cyclotron Laboratory (NSCL) of Michigan State University. A beam of 140 MeV/nucleon ^{48}Ca was accelerated by the Coupled Cyclotron Facility (CCF) and directed onto a 987 mg/cm^2 ^{9}Be fragmentation target at the mid-acceptance position of the A1900 fragment separator [10]. Two cocktail beams consisting of several projectile fragments each were selected by the $B\rho$–ΔE–$B\rho$ method and delivered to the S800 analysis line, which was operated in focused mode [11]. The first setting included $^{38–40}$Si; ^{36}Si was a member of the second cocktail beam.

The charge and magnetic rigidity of incoming projectiles were determined on an event-by-event basis by measuring the energy loss through a Si-PIN detector and the dispersive angle through a pair of tracking PPACs. Projectiles were directed onto a RIKEN–Kyushu–Rikkyo liquid hydrogen (LH_2) target [12] placed at the target position of the S800 spectrograph. The average thickness of hydrogen intercepted by the beam was 10.4(2) mm; the combined thickness of the aluminum entrance and exit windows was 0.42(2) mm. The spectrograph was set to accept (in)elastically scattered beam particles in the S800 focal plane [13]. Energy loss in an ion chamber and dispersive position measured by a cathode readout drift chamber, both in the focal plane of the S800 spectrograph, determined the charge and magnetic rigidity of heavy reaction residues exiting the target. Time of flight was measured between timing scintillators placed at the exit of the A1900 and in the S800 focal plane and was corrected by the measured momentum and flight path on an event-by-event basis. A combination of momentum measurements and time-of-flight information allowed unambiguous mass determination of projectiles exiting the target.

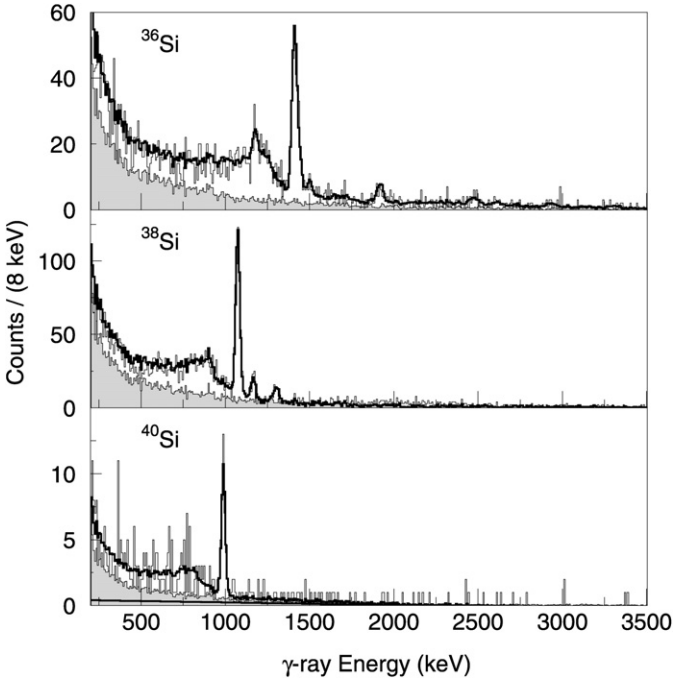

Fig. 1. Doppler-corrected spectra of γ rays in prompt coincidence with inelastically scattered ^{36,38,40}Si. Projectile velocities were approximately $0.4c$. The fit function and particle-scaled background are superimposed on each spectrum as a thick black line and a grey shaded region, respectively.

Excitation cross sections for inelastic proton scattering to specific excited states were determined using the thick-target, γ-ray tagging method [14]. Projectile nuclei which were excited by inelastic scattering off protons in the LH_2 target cell decayed in-flight by emitting γ rays. The spectrum of γ rays detected in coincidence with each nucleus is then a measure of the total inelastic excitation cross section to individual bound states. Because γ rays do not suffer energy straggling, experiments may utilize thick targets without loss of resolution. In turn, the use of thick targets enables measurements on exotic nuclei with low production rates. In this experiment, sixteen 32-fold segmented SeGA detectors [15] were placed around the LH_2 target in two rings at 37° and 90° from the beam axis. The detector segmentation enabled event-by-event Doppler correction of the γ-ray spectra measured in coincidence with reaction residues identified in the S800 focal plane.

Doppler-corrected spectra for inelastically scattered ^{36,38,40}Si are shown in Fig. 1. A prompt particle-γ coincidence window of 60 ns was used to reduce the random coincidence contribution to the spectra. Thick-target, inverse-kinematics experiments are typically subject to a γ-ray background resulting from beam-target interactions. In the case of a liquid hydrogen target, these beam-target interactions come mostly from reactions in the aluminum target windows. This background was measured by collecting data with the liquid hydrogen removed from the target cell and the S800 spectrograph adjusted to account for the lower energy loss of the beam through the empty cell. This empty-target background was scaled for each

spectrum by the number of downscaled beam particles in the associated particle identification gate. In Fig. 1, scaled backgrounds are shaded and superimposed on the spectra taken in the reaction setting; fits are overlaid as thick lines. In each spectrum, the $2_1^+ \rightarrow 0_1^+$ transition is the dominant peak. The energy separation between the $4_1^+ \rightarrow 2_1^+$ and $2_1^+ \rightarrow 0_1^+$ transitions in ^{36}Si was fixed using the γ-ray energies reported by Liang et al. [6]. In the case of ^{40}Si, an additional linear background function was found to improve the fit and has been superimposed as a thick line.

For each nucleus, the fitted number of emitted γ rays was combined with the number of target protons per unit area and the number of downscaled particles in the relevant particle identification gate to obtain cross sections for the population of individual final states. Level schemes were deduced from energy sums and coincidence relations found in this and other reactions for ^{36,38}Si. Decay schemes deduced in this experiment will be discussed in a separate article. Feeding contributions were then subtracted from the total cross section for each $2_1^+ \rightarrow 0_1^+$ transition to obtain the inelastic proton excitation cross section, $\sigma_{0_1^+ \rightarrow 2_1^+}$. Table 1 lists the uncorrected cross section, the feeding correction due to transitions placed in the decay scheme, the feeding estimate applied due to unplaced transitions, and feeding-corrected excitation cross section for ^{36,38,40}Si. The unplaced feeding estimate was taken as 50(25)% of the summed strength of all unplaced γ-ray transitions. No feeding transitions were observed in ^{40}Si. An estimated 20% unobserved feeding contribution was included in the calculation of the cross-section uncertainty for ^{40}Si. This is approximately the level of feeding observed in ^{38}Si, and a feeding transition of this strength might be missed due to the low statistics. The aluminum target windows account for 5.7(2)% of the atom fraction of the LH_2 target cell. Therefore, their contribution to measured excitation cross sections is negligible. Spherical tensors and differential cross sections from ECIS97 [16] calculations were used to estimate the effect of γ-ray angular distributions and reaction-channel gating on the final cross section. The combined correction for these effects was 2–3%.

Due to the strong proton subshell closure at $Z = 14$ [7,9], a coupling of proton and neutron excitations yielding strong static deformation is not expected [17]. Furthermore, Liang et al. have measured the ratio ($R_{4/2}$) of $E(4_1^+)$ to $E(2_1^+)$ to be 2.02 in ^{36}Si, providing evidence of vibrational collectivity in ^{36}Si [6,18], and recent mass measurements find that no evidence of static deformation in ^{36,38,40}Si [19]. Thus, we have used a vibrational form factor to describe the $0_1^+ \rightarrow 2_1^+$ excitation in ^{36,38,40}Si. ECIS97 [16] was used with the global optical model parameterization of Koning and Delaroche [20] to deduce deformation parameters. For ^{36,38}Si, the deformation parameter of each charge distribution, $|\beta_{2C}|$, was taken from Coulomb excitation measurements [5], and the deformation parameter of the mass distribution, which we will call $|\beta_{2,(p,p')}|$, was varied to reproduce the measured excitation cross sections.

Because no Coulomb excitation measurement exists for ^{40}Si, we have chosen to require the charge and mass distributions to share a common deformation length, $\delta_C = \delta_{(p,p')}$, where

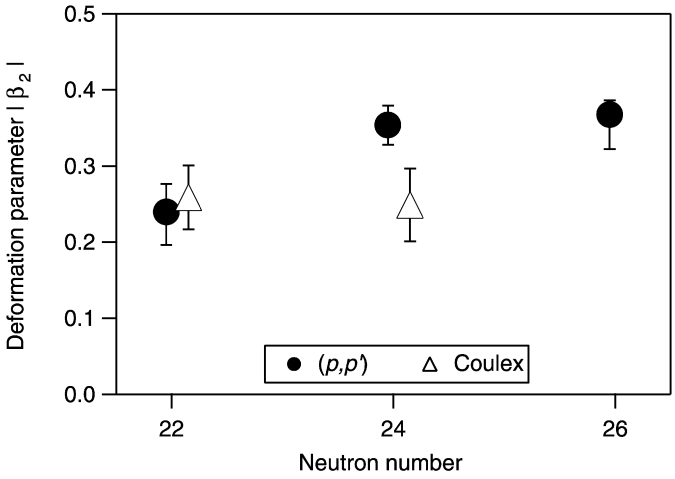

Fig. 2. Deformation parameters $|\beta_{2,(p,p')}|$ and previously measured $|\beta_{2,C}|$ [5] are plotted against neutron number for the nuclei ^{36,38,40}Si.

$\delta = \beta R$ and $R = r_0 A^{1/3}$. The optical model parameterization [20] gives mass dependent r_0 values of 1.181, 1.183, and 1.185 fm for ^{36,38,40}Si, respectively. An r_0 value of 1.2 fm was used for the deformation of the charge distribution [21]. As before, the deformation parameter was varied to reproduce the measured excitation cross section. To measure the effect of this unknown Coulomb deformation parameter on the extracted $|\beta_{2,(p,p')}|$ value, this calculation was repeated using instead the measured $|\beta_{2C}|$ value of ^{38}Si. Although the second calculation uses a $|\beta_{2C}|$ value 36% smaller than the one obtained by requiring a common deformation length, the extracted $|\beta_{2,(p,p')}|$ values differ by less than 2%. This difference is negligible. Table 1 presents the deformation parameters extracted in this experiment using vibrational form factors. Results are also shown for $|\beta_{2,(p,p')}|$ values extracted assuming positive and negative static deformations with axial symmetry.

Fig. 2 shows $|\beta_{2,(p,p')}|$ as a function of neutron number for the even–even silicon isotopes along with the corresponding deformation parameters for ^{36,38}Si deduced from a prior Coulomb excitation experiment, $|\beta_{2C}|$. If both $N = 20$ and $N = 28$ had large shell gaps in the silicon isotopes, one would expect maximum collectivity at midshell, ^{38}Si, and ^{36,40}Si would have a similar, lower level of collectivity. Instead, the observed asymmetry between the beginning and end of the neutron $0f_{7/2}$ shell indicates greater collectivity at $N = 26$ than at $N = 22$ in the silicon isotopes. In the sulfur isotopes a similar pattern of increased collectivity has been observed approaching $N = 28$. However, the enhanced collectivity found in the sulfur chain derives, in part, from the narrowing of the proton $1s_{1/2}$–$0d_{3/2}$ subshell gap. This leads to both enhanced proton collectivity and coupling between collective proton and neutron excitations culminating in a rotational structure in ^{42}S, with $R_{4/2} \sim 3.0$ [18,22]. Because the $Z = 14$ subshell closure is known to be large at $N = 28$ [7,9], the increased collectivity observed in ^{40}Si cannot be attributed to proton excitations or a coupling of proton and neutron excitations. Valence protons are prevented from contributing to the onset of collectivity in silicon, thus the increased collectivity observed in ^{40}Si is due only to neutron excitations across the $N = 28$ shell gap.

Table 1
Inelastic proton-scattering cross sections and deformation parameters deduced in the current experiment are given for ^{36,38,40}Si. Cross sections are listed for: the 2_1^+ state before feeding corrections, a feeding correction for transitions placed in the decay scheme, a feeding correction equal to 50(25)% of the unplaced transition strength, and the 2_1^+ state after feeding corrections. Quadrupole deformation parameters deduced using the following collective model form factors are also listed: vibrational, prolate rotational, and oblate rotational

N	$\sigma_{0_1^+\to 2_1^+}$ (mb)				$\lvert\beta_{2,(p,p')}\rvert$		
	Uncorrected	Feeding (placed)	Feeding (unplaced)	Feeding corrected	Vibrational	Prolate	Oblate
22	19.2(10)	7.6(11)	4.2(21)	7.3(25)	0.24(4)	0.23^{+3}_{-4}	0.25^{+4}_{-5}
24	19.6(20)	2.7(4)	1.5(7)	15.4(23)	0.35^{+2}_{-3}	0.34^{+2}_{-3}	0.38(3)
26	20.2(21)	0.0	0.0^{+42}_{-0}	20.2^{+21}_{-47}	0.37^{+2}_{-5}	0.35^{+2}_{-4}	0.39^{+2}_{-5}

Table 2
Deformation parameters deduced in the current experiment ($\lvert\beta_{2,(p,p')}\rvert$) using a vibrational form factor, deformations from previous Coulomb excitation measurement ($\lvert\beta_{2C}\rvert$) [5], shell-model matrix elements A_p and A_n, and experimental and shell-model $(\frac{M_n}{M_p})/(\frac{N}{Z})$ ratios are given for ^{36,38,40}Si

N	$\lvert\beta_{2,(p,p')}\rvert$	$\lvert\beta_{2C}\rvert$	A_p (fm)	A_n (fm)	$(\frac{M_n}{M_p})/(\frac{N}{Z})_{\text{expt}}$	$(\frac{M_n}{M_p})/(\frac{N}{Z})_{\text{SM}}$
22	0.24(4)	0.26(4)	5.44	13.1	0.88^{+27}_{-29}	0.90
24	0.35^{+2}_{-3}	0.25(5)	5.04	19.7	1.52(37)	0.96
26	0.37^{+2}_{-4}	–	5.28	23.5	–	0.92

By comparing deformation parameters deduced from inelastic proton scattering to those from Coulomb excitation, the neutron and proton collective contributions may be compared. A simple collective model for low-lying collective excitations would assign a common deformation to both neutrons and protons, with the ratio of matrix elements determined simply by the number of each nucleon (i.e., $\frac{M_n}{M_p} = \frac{N}{Z}$). To better compare isotopes, we normalize the ratio of neutron to proton matrix elements by the ratio N/Z for each isotope. In a single closed-shell nucleus, the collective strength of the closed-shell nucleons is attenuated relative to open-shell valence nucleons [23]. Thus, the silicon nuclei studied here, each consisting of a closed proton shell plus valence neutrons, would be expected to have ratios $(\frac{M_n}{M_p})/(\frac{N}{Z}) > 1$ in this model.

Table 2 lists the deformation parameters deduced here using inelastic proton scattering and the values deduced previously in Coulomb excitation [5]. While Coulomb excitation probes proton matrix elements only, proton scattering is sensitive to both proton and neutron degrees of freedom. The ratio of interaction strengths for protons interacting with neutrons and protons within a nucleus, b_n/b_p, is a function of bombarding energy. At low proton energies (10–50 MeV), b_n/b_p is approximately 3, and near 1 GeV, b_n/b_p is 1 [24]. The present study takes place in inverse kinematics with mid-target beam energies of 90–100 MeV/nucleon, corresponding to 90–100 MeV protons in forward-kinematics. Based on nucleon–nucleon effective interactions [25,26], we adopt the value $b_n/b_p = 1.45(20)$. The radial form factors of the transition densities are different for protons and neutrons, because valence protons (*sd*) and neutrons (*pf*) occupy different major shells. This increases the sensitivity of our deduced deformation parameter to neutrons. We estimate this increases the effective b_n/b_p by 34(17)% for ^{36}Si and 43(22)% for ^{38}Si. This change leads to less than a 5% correction in $(\frac{M_n}{M_p})/(\frac{N}{Z})$ for these isotopes. The experimental ratios of matrix elements have been calculated using Eq. (1) [27] and are listed in Table 2.

$$\frac{M_n}{M_p} = \frac{b_p}{b_n}\left[\frac{\delta_{(p,p')}}{\delta_C}\left(1 + \frac{b_n}{b_p}\frac{N}{Z}\right) - 1\right]. \tag{1}$$

We note that ^{38}Si is consistent with $(\frac{M_n}{M_p})/(\frac{N}{Z}) > 1$ and that the addition of two $0f_{7/2}$ neutrons substantially increases the neutron collectivity at $N = 24$.

These data were then compared with values calculated in the shell model. Shell-model calculations were performed in OXBASH [28] (for ^{36}Si) and CMICHSM [29] (for ^{38,40}Si) in a $\pi(sd)^{Z-8}\nu(pf)^{N-20}$ model space using the updated interaction of Nowacki and collaborators [30,31]. The proton and neutron quadrupole matrix elements for the $0_1^+ \to 2_1^+$ excitation in each nucleus were calculated in the generalized effective charge model [32]; $M_p = A_p(1 + \delta_{pp}) + A_n\delta_{pn}$ and $M_n = A_n(1 + \delta_{nn}) + A_p\delta_{np}$. Here A_n and A_p are the quadrupole matrix elements for valence particles in the model space; the calculated $A_{n,p}$ values are listed in Table 2. The coupling of valence excitations to core excitations beyond the model space is handled through the polarization charges, δ.

For this analysis, we began with the simplifying assumption that $\delta_{pp} = \delta_{nn}$ and $\delta_{pn} = \delta_{np}$. Three sets of polarization charges $(\delta_{pp}, \delta_{pn})$ were tested: (0.5, 0.5), (0.2, 0.8), and (0.2, 0.5). The first of these pairs represents the standard isoscalar choice. The second pair has a significant isovector component, which has been suggested in the *pf* shell [33]. The third pair are the accepted polarization charges for the *sd* shell [34]. Both the standard isoscalar polarization charges and the set suggested for the *pf* shell overpredict the measured $B(\text{E2}; 0_1^+ \to 2_1^+)$ value in ^{38}Si [5]. The standard *sd*-shell effective charges yield 1σ agreement with the measured ^{36,38}Si $B(\text{E2}\uparrow)$ values and have been used to calculate the shell-model $(\frac{M_n}{M_p})/(\frac{N}{Z})$ ratios given in Table 2. The experimental and shell-model $(\frac{M_n}{M_p})/(\frac{N}{Z})$ ratios are

in agreement for ^{36}Si, but ^{38}Si exhibits more neutron collectivity than the shell model predicts. We also compared the data against the Bohr–Mottelson (BM) effective charge model, given in Eq. 6-386a of [35], extending the model to handle polarization of core neutrons by valence nucleons. The $B(\mathrm{E2}\uparrow)$ values and $(\frac{M_n}{M_p})/(\frac{N}{Z})$ trend obtained using the BM effective charges were essentially the same as was found using *sd*-shell effective charges. However, $(\frac{M_n}{M_p})/(\frac{N}{Z})$ calculated using the BM effective charges were ∼20% higher, giving somewhat better agreement with experiment.

The potential discrepancy between observed and calculated neutron collectivity in ^{38}Si could be explained in three different ways: (i) a deficiency in the shell model, such as a too-large $N = 28$ shell gap; (ii) an enhanced core neutron—valence neutron coupling; or (iii) an overestimation of $|\beta_{2,(p,p')}|$ due to the formation of a neutron skin. The latter two possibilities have also been suggested to explain enhanced neutron collectivity observed in ^{38,40}S [36,37]. While the thick-target, γ-ray tagging method enables collectivity studies in very-neutron rich systems, it is not sensitive to the proton angular distributions needed to test the shape of the nuclear potential. Precision measurements sensitive to details of the angular distribution—such as the inverse-kinematics proton scattering studies of ^{40,42}Ar [38] and ^{38,40}S [37,39]—will be needed to investigate possible neutron skins in this region. Microscopic calculations of polarization charges and Coulomb excitation experiments taking advantage of the higher exotic beam rates now available are needed to fully understand the evolution of collectivity near $N = 28$. A Coulomb excitation measurement with 10% uncertainty on the measured $B(\mathrm{E2}\uparrow)$ values would reduce the uncertainty in the $(\frac{M_n}{M_p})/(\frac{N}{Z})$ ratios by 25% for ^{36}Si and 57% for ^{38}Si.

In conclusion, proton inelastic excitation cross sections, $\sigma_{0_1^+\to 2_1^+}$, have been measured in the neutron-rich nuclei ^{36,38,40}Si. Quadrupole deformation parameters, $|\beta_{2,(p,p')}|$, have been deduced and show an asymmetry about midshell, $N = 24$. The strong $Z = 14$ subshell gap in silicon isotopes links the enhanced collectivity at $N = 26$ directly to a narrowing of the $N = 28$ shell gap at $Z = 14$. Relative neutron and proton contributions to collectivity indicate a rise in neutron collectivity observed at $N = 24$. This suggests the need for future, differential cross-section measurements to quantitatively understand neutron collectivity approaching $N = 28$.

Acknowledgements

This work was supported by the National Science Foundation under Grants No. PHY-0606007, PHY-9875122, PHY-0555366, PHY-0355129, INT-0089581 and by the Japan Society for the Promotion of Science.

References

[1] C. Thibault, et al., Phys. Rev. C 12 (1975) 644.
[2] X. Campi, et al., Nucl. Phys. A 251 (1975) 193.
[3] E.K. Warburton, J.A. Becker, B.A. Brown, Phys. Rev. C 41 (1990) 1147.
[4] T. Glasmacher, et al., Phys. Lett. B 395 (1997) 163.
[5] R.W. Ibbotson, et al., Phys. Rev. Lett. 80 (1998) 2081.
[6] X. Liang, et al., Phys. Rev. C 74 (2006) 014311.
[7] P. Doll, et al., Nucl. Phys. A 263 (1976) 210.
[8] P.D. Cottle, K.W. Kemper, Phys. Rev. C 58 (1998) 3761.
[9] J. Fridmann, et al., Nature 435 (2005) 922; J. Fridmann, et al., Phys. Rev. C 74 (2006) 034313.
[10] D.J. Morrissey, et al., Nucl. Instrum. Methods Phys. Res. B 204 (2003) 90.
[11] D. Bazin, et al., Nucl. Instrum. Methods Phys. Res. B 204 (2003) 629.
[12] H. Ryuto, et al., Nucl. Instrum. Methods Phys. Res. A 555 (2005) 1.
[13] J. Yurkon, et al., Nucl. Instrum. Methods Phys. Res. A 422 (1999) 291.
[14] H. Iwasaki, et al., Phys. Lett. B 481 (2000) 7.
[15] W.F. Mueller, et al., Nucl. Instrum. Methods Phys. Res. A 466 (2001) 492.
[16] J. Raynal, Coupled channel code ECIS97, also Notes on ECIS94, Note CEA-N-2772 (1994).
[17] E. Caurier, F. Nowacki, A. Poves, Nucl. Phys. A 742 (2004) 14.
[18] R.F. Casten, Nuclear Structure from a Simple Perspective, Oxford Univ. Press, New York, 2000.
[19] B. Jurado, et al., Phys. Lett. B 649 (2007) 43.
[20] A.J. Koning, J.-P. Delaroche, Nucl. Phys. A 13 (2003) 231.
[21] S. Raman, C.W. Nestor Jr., P. Tikkanen, At. Data Nucl. Data Tables 78 (2001) 1.
[22] D. Sohler, et al., Phys. Rev. C 66 (2002) 054302.
[23] A.M. Bernstein, V.R. Brown, V.A. Madsen, Phys. Lett. B 103 (1981) 255.
[24] A.M. Bernstein, V.R. Brown, V.A. Madsen, Comments Nucl. Part. Phys. 11 (1983) 203.
[25] J.A. Carr, F. Petrovich, J.J. Kelly, AIP Conf. Proc. 124 (1985) 230.
[26] M.A. Franey, W.G. Love, Phys. Rev. C 31 (1985) 488.
[27] L.A. Riley, et al., Phys. Rev. C 72 (2005) 024311.
[28] B.A. Brown, et al., OXBASH for Windows, MSU-NSCL Report No. 1289 (2004).
[29] M. Horoi, CMICHSM, Advanced Computational Methods for Solving the Nuclear Many-Body Problem, Institute for Nuclear Theory, Seattle, WA, 2002, http://www.int.washington.edu/talks/WorkShops/ACD02.
[30] J. Retamosa, E. Caurier, F. Nowacki, A. Poves, Phys. Rev. C 55 (1997) 1266.
[31] S. Nummela, et al., Phys. Rev. C 63 (2001) 044316.
[32] B.A. Brown, B.H. Wildenthal, Phys. Rev. C 21 (1980) 2107.
[33] R. du Rietz, et al., Phys. Rev. Lett. 93 (2004) 222501.
[34] H. Sagawa, B.A. Brown, Nucl. Phys. A 430 (1984) 84.
[35] A. Bohr, B.R. Mottelson, Nuclear Structure, vol. II, W. A. Benjamin, New York, 1975.
[36] N. Alamanos, F. Auger, B.A. Brown, A. Pakou, J. Phys. G 24 (1998) 141.
[37] F. Maréchal, et al., Phys. Rev. C 60 (1999) 034615.
[38] H. Scheit, et al., Phys. Rev. C 63 (2000) 014604.
[39] J.H. Kelley, et al., Phys. Rev. C 56 (1997) R1206.